Optimal Selective Harmonic Control for Power Harmonics Mitigation

Zhou, Keliang; Yang, Yongheng; Blaabjerg, Frede; Wang, Danwei

Published in:
IEEE Transactions on Industrial Electronics

DOI (link to publication from Publisher):
10.1109/TIE.2014.2336629

Publication date:
2015

Document Version
Early version, also known as pre-print

Optimal Selective Harmonic Control for Power Harmonics Mitigation

Keliang Zhou, *Senior Member, IEEE*, Yongheng Yang, *Student Member, IEEE*, Frede Blaabjerg, *Fellow, IEEE*, Danwei Wang, *Senior Member, IEEE*

***Abstract* — This paper proposes an Internal Model Principle (IMP) based optimal Selective Harmonic Controller (SHC) for power converters to mitigate power harmonics. According to the harmonics distribution caused by power converters, a universal recursive SHC module is developed to deal with a featured group of power harmonics. The proposed optimal SHC is of hybrid structure: all recursive SHC modules with weighted gains are connected in parallel. It bridges the real "*nk±m order RC*" and the complex "parallel structure RC". Compared to other IMP based control solutions, it offers an optimal trade-off among the cost, the complexity and the performance: high accuracy, fast transient response, easy-implementation, cost-effective, and also easy-to-design. The analysis and synthesis of the optimal SHC system are addressed. The proposed SHC offers power converters a tailor-made optimal control solution for compensating selected harmonic frequencies. Application examples of grid-connected inverters confirm the effectiveness of the proposed control scheme.**

***Index Terms* — internal model principle, power converter, power system harmonics, repetitive control, resonant control**

I. Introduction

IN PRACTICAL electrical power systems, power harmonics caused by power converters interfaced loads and distributed generators usually concentrate on some particular frequencies [1]-[7], e.g. single-phase H-bridge converters mainly produce $4k\pm1$ (k=1,2,…) order power harmonics; n-pulse (n=6,12,…) converters based HVDC transmission systems mainly produce $nk\pm1$ (k=1,2,…) order power harmonics. To dealing with power harmonics issues, power converters demand optimal control strategies, which can compensate power harmonics with high control accuracy while maintaining fast transient response, guaranteeing robustness, and being feasible for implementation [1]-[4].

Manuscript received February 23, 2014; revised May 19, 2014; accepted June 10, 2014.

K. Zhou is with the Department of Electrical and Computer Engineering, The University of Canterbury, Christchurch 8041, New Zealand (e-mail: eklzhou@ieee.org).

Y. Yang and F. Blaabjerg are with the Department of Energy Technology, Aalborg University, DK-9220 Aalborg, Denmark (e-mail: yoy@et.aau.dk; fbl@et.aau.dk).

D. Wang is with the Division of Control and Instrumentation, School of Electrical and Electronic Engineering, Nanyang Technological University, Singapore 639798, Singapore (email: edwwang@ntu.edu.sg).

Color versions of one or more of the figures in this paper are available online at http://ieeexplore.ieee.org.

Digital Object Identifier: 10.1109/TIE.2014.xxxxxx

According to the Internal Model Principle (IMP) [5], [6], zero error tracking of any reference input in steady-state, can be accomplished if a generator of the reference input is included in a stable closed-loop system. IMP-based classical Repetitive Control (RC) [4]-[21] and Resonant Control (RSC) [2], [3], [22]-[26] provide very simple but effective control solutions to power harmonics compensation. However, without taking the harmonics distribution into consideration, recursive RC can compensate all harmonics, but typically yields slow total convergence rate; considering the harmonics distribution, a parallel combination of Multiple Resonant Controllers (MRSC) at selected harmonic frequencies can render quite fast transient response, but would cause heavy parallel computation and design complexity in dealing with a large number of harmonics. Discrete Fourier Transformation (DFT) based RC [2], [7] is virtually equivalent to MRSC, and it can flexibly and selectively compensate the desired harmonics. Unlike MRSC, its identified feature is that the computational complexity is independent of the number of selected harmonics to be compensated. Nonetheless, DFT based RC, which is in the form of FIR filter, would involve a large amount of parallel computation that is proportional to the number of samples per fundamental period, and thus it is especially suitable for high performance fixed-point DSP implementation. Moreover, based on IMP, odd harmonic RC and $6l\pm1$ RC, which are in the recursive form, are introduced in [8], [9]. The two RC controllers offer an accurate, fast, and feasible selective harmonic compensation solution for power converters to specially compensate odd order harmonics and $6l\pm1$ order harmonics respectively. However, a universal Selective Harmonic Control (SHC) for optimal power harmonics compensation is still an open issue.

In this paper, an optimal SHC has been proposed to address above issues. The selected harmonic frequencies have been classified into a limited number of clusters. A generic recursive SHC module is developed to exclusively incorporate the internal models for each cluster of harmonics. All the recursive SHC modules are connected in parallel to form a complete Optimal SHC (OSHC) controller, where each SHC module has an individual and independent control gain. The analysis and synthesis of OSHC systems are also addressed. Finally, OSHC is applied to PWM converters for case studies.

II. Optimal Selective Harmonic Control

In this section, an OSHC scheme has been developed for power converters to mitigate power harmonics after a comprehensive analysis of mainstream IMP-based harmonic controllers, such as the classical RC, the MRSC and the DFT-based RC.

A. Classical Repetitive Control

As shown in Fig. 1, a Classical RC (CRC) can be written as

$$G_{rc}(s)=\frac{u_{rc}(s)}{e(s)}=\frac{k_{rc}\cdot e^{-s(T_o-T_1)}}{1-e^{-sT_o}}=\frac{k_{rc}\cdot e^{-sT_0}}{1-e^{-sT_o}}e^{sT_c} \quad (1)$$

where k_{rc} is the control gain; $T_o=2\pi/\omega_o=1/f_o$ is the fundamental period of signals with f_o being the fundamental frequency, ω_o being the fundamental angular frequency; and T_c is the lead phase compensation time. Recursive CRC of (1) only consumes a little computation in its implementation. The transient response is subject to the delay time T_0.

The transfer function of RC in (1) can be expanded as [13],

$$G_{rc}(s)=k_{rc}\left[\overbrace{-\frac{1}{2}}^{\text{Proportional}}+\overbrace{\frac{1}{T_0 s}}^{\text{Integrator}}+\overbrace{\frac{1}{T_o}\sum_{n=1}^{\infty}\frac{2s}{s^2+(n\omega_0)^2}}^{\text{RSC}}\right]e^{sT_c} \quad (2)$$

which indicates that the CRC is equivalent to the parallel combination of a proportional gain, an integrator and all RSC controllers at harmonic frequencies (*i.e.* the internal models of DC and all harmonics). According to IMP, infinity gains at harmonic frequencies $n\omega_0$ for all RSC components enable CRC to compensate all harmonics. It is known that the error convergence rate of CRC is proportional to its control gain k_{rc} [17], [18]. Since the equivalent gains for all RSC components are identical (*i.e.* $2k_{rc}/T_0$), it is impossible for CRC to optimize its transient response by tuning the control gains independently at selected harmonic frequencies.

Most modern controllers are implemented in digital form. For a plug-in digital CRC system shown in Fig. 2, where $Q(z)$ is a low-pass filter and $G_f(z)$ is a phase lead compensator, the stability range of control gain k_{rc} is derived as follows [17],

$$0<k_{rc}<\frac{2\cos\left\{\theta_h(e^{j\omega})+\theta_f(e^{j\omega})\right\}}{N_h(e^{j\omega})N_f(e^{j\omega})} \quad (3)$$

in which $H(z)=G_c(z)G_p(z)/(1+G_c(z)G_p(z))$ with $N_h(e^{j\omega})$ and $\theta_h(e^{j\omega})$ being magnitude-frequency characteristics of $H(z)$ and phase-frequency characteristics of $H(z)$ respectively; $N_f(e^{j\omega})$ and $\theta_f(e^{j\omega})$ are magnitude-frequency characteristics of $G_f(z)$ and phase-frequency characteristics of $G_f(z)$ respectively. If $G_f(z)H(z)=1$, *i.e.* $\theta_h(e^{j\omega})+\theta_f(e^{j\omega})=0$ for all ω below Nyquist frequency, the stability range of the control gain k_{rc} will be [8]

$$0<k_{rc}<2 \quad (4)$$

When $\theta_h(e^{j\omega})+\theta_f(e^{j\omega})=0$, zero phase compensation is achieved, it not only leads to a larger stability range of k_{rc} and thus a faster transient response, but also significantly simplifies the design of RC system. However, due to parameter variations and un-modeled uncertainties, an accurate transfer function of $H(z)$ is unavailable. Therefore, it is difficult to obtain zero phase compensation for RC systems, especially in the high frequency band. In practice, a simple but effective phase lead compensator $G_f(z)=z^m$ can be adopted, and it will significantly contribute to the improvement of the system stability, the steady-state accuracy and the transient response [17], [18]. Moreover, a low-pass filter $Q(z)$ is introduced to improve the control system stability at the cost of reduced tracking accuracy in high frequency band. $Q(z)$ brings a trade-off between control accuracy and system robustness.

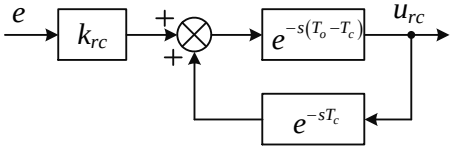

Fig. 1. Classical Repetitive Controller $G_{rc}(s)$.

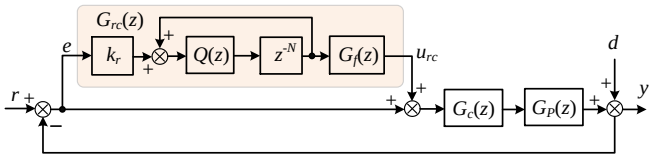

Fig. 2. Plug-in repetitive control system.

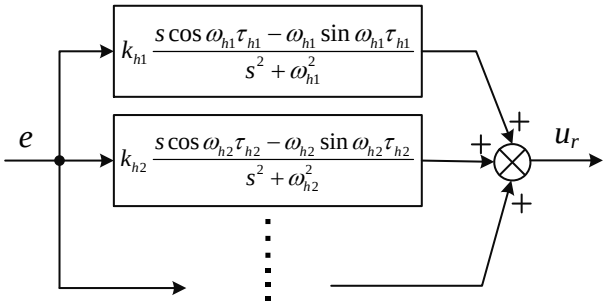

Fig. 3. Multiple resonant controller $R(s)$.

From (1)-(4), it is clear that, CRC offers slow transient response because the control gains at all harmonic frequencies are identical and limited. The CRC, $G_{rc}(z)$, will take only a few computation steps to update its output online.

B. Multiple Resonant Control

To speed up the transient response while maintaining satisfactory accuracy, a parallel combination of multiple resonant controllers (MRSC) at selected harmonic frequencies can be used to replace RC to compensate major harmonics as follows [2], [3], [22], [23],

$$R(s)=\sum_{h\in N_h}k_h\frac{s\cos\omega_h\tau_h-\omega_h\sin\omega_h\tau_h}{s^2+\omega_h^2}=\sum_{h\in N_h}R_h(s) \quad (5)$$

where $R_h(s)$ is the RSC component at harmonic frequency ω_h with the gain k_h; τ_n is the phase lead compensation time at ω_h. In contrast to RC of (1), each RSC component in MRSC of (5) can independently choose its gain k_h and phase lead compensation time τ_n so as to optimize its transient response. Large gains at large harmonic frequencies will lead to faster transient response. Moreover, the more RSC components are added, the higher accuracy can be achieved by MRSC. However, each RSC component in (5) is corresponding to only one harmonic frequency. Consequently, MRSC of (5) will yield heavy parallel computation burden and tuning difficulties if many RSC components are embedded.

C. DFT-based Repetitive Control

A digital SHC named DFT-based RC, is shown in Fig. 3 [2], [7], where the DFT filter $F_{DFT}(z)$ can be expressed as

$$F_{DFT}(z)=\sum_{h\in N_h}F_{dh}(z)$$
$$=\frac{2}{N}\sum_{i=0}^{N-1}\left(\sum_{h\in N_h}\cos\left[\frac{2\pi}{N}h\left(i+N_a\right)\right]\right)z^{-i}=\frac{2}{N}\sum_{i=0}^{N-1}\vartheta_i z^{-i} \quad (6)$$

in which i, N, h, N_h and N_a represent the ith sample point, number of samples per fundamental period, harmonic order, the set of selected harmonic frequencies, and the number of leading steps for phase-lead compensation [7].

And the corresponding DFT-based RC can be written as

$$G_{DFT}(z)=\frac{u_F(z)}{e(z)}=\frac{k_F F_{DFT}(z)}{1-F_{DFT}(z)z^{-N_a}}=\frac{k_F\sum_{h\in N_h}F_{dh}(z)}{1-z^{-N_a}\sum_{h\in N_h}F_{dh}(z)} \quad (7)$$

which is approximately equivalent to the MRSC of (5) [3],[7].

Therefore only a change of the coefficients of the FIR filter of (6) is required for the compensation of more or less harmonics without any additional calculation. Obviously, DFT-based RC provides flexible selective harmonic compensation, and its computational complexity is independent of the number of selected harmonics to be compensated. However, DFT-based RC would involve a large amount of parallel computation that is proportional to N for the filter $F_{FDT}(z)$ of (6), and thus it is suitable for high performance fixed-point DSP implementation.

D. Proposed Selective Harmonic Control

It is clear that, better SHC solution should make an optimal tradeoff among the above three IMP-based control solutions: fast transient response, high accuracy and robustness, light computation, and easy implementation.

Since power harmonics produced by power converters usually concentrate on $nk\pm1$ (k=0, 1, 2, …) order harmonic frequencies. To compensate selected $nk\pm m$ (k=0, 1, 2, … and $m<n$) order harmonics, a universal SHC module which only include the internal models of $nk\pm m$ order harmonics, can be generated as

$$G_{nm}(s)=\frac{k_m}{2}\left(\frac{e^{\frac{-sT_0}{n}+j\frac{2\pi m}{n}}}{1-e^{\frac{-sT_0}{n}+j\frac{2\pi m}{n}}}+\frac{e^{\frac{-sT_0}{n}+j\frac{2\pi m}{n}}}{1-e^{\frac{-sT_0}{n}+j\frac{2\pi m}{n}}}\right)e^{sT_1}$$
$$=k_m\frac{\cos\left(2\pi m/n\right)e^{\frac{sT_o}{n}}-1}{e^{\frac{2sT_o}{n}}-2\cos\left(2\pi m/n\right)e^{\frac{sT_o}{n}}+1}e^{sT_c} \quad (8)$$

where T_o, f_o, ω_o, and T_c have been defined previously, n and m are integers with $n>m\geq0$. Since

$$\frac{e^{-2\pi\left(\frac{s}{n\omega_o}\pm\frac{jm}{n}\right)}}{1-e^{-2\pi\left(\frac{s}{n\omega_o}\pm\frac{jm}{n}\right)}}$$
$$=-\frac{1}{2}+\frac{n}{T_o}\frac{1}{\left(s\pm jm\omega_o\right)}+\frac{n}{T_o}\sum_{k=1}^{+\infty}\frac{2\left(s\pm jm\omega_o\right)}{\left(s\pm jm\omega_o\right)^2+n^2k^2\omega_o^2} \quad (9)$$

where k=0, 1,2,… and m=0,1,2,…,n-1. From (8) and (9), it is clear that complex SHC modules of (9) with equal gains are successfully combined into a real SHC one of (8). SHC Module of (8) is equivalent to a parallel combination of RSC at $nk\pm m$ order harmonic frequencies. According to IMP, the SHC module of (8) can achieve zero tracking error exclusively at selected $nk\pm m$ order harmonic frequencies without the heavy parallel computation burden. From (8) and (9), it is known that the equivalent gain at $nk\pm m$ order harmonic frequencies is nk_m/T_0. Since the convergence rate of any RSC is proportional to its gain [23], compared with CRC of (2), the error convergence rate at $nk\pm m$ order harmonic frequencies of SHC module of (8) can be n/2 times faster if $k_m=k_{rc}$.

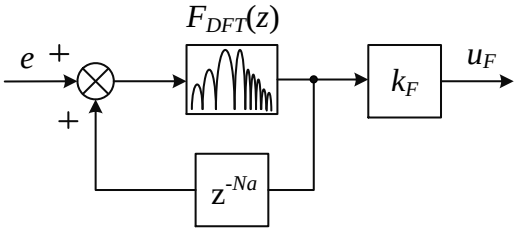

Fig. 4. DFT-based repetitive controller $G_{DFT}(z)$.

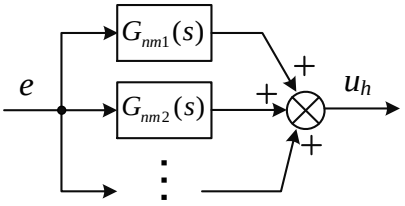

Fig. 5. Proposed selective harmonic controller $G_{SHC}(s)$.

In practical applications, modified SHC modules $G_{nm}(s)$ will be employed as

$$G_{nm}(s)$$
$$=\frac{k_m G_f(s)}{2}\left(\frac{e^{\frac{-sT_0}{n}+j\frac{2\pi m}{n}}Q(s)}{1-e^{\frac{-sT_0}{n}+j\frac{2\pi m}{n}}Q(s)}+\frac{e^{\frac{-sT_0}{n}-j\frac{2\pi m}{n}}Q(s)}{1-e^{\frac{-sT_0}{n}-j\frac{2\pi m}{n}}Q(s)}\right) \quad (10)$$
$$=k_m G_f(s)\frac{\cos\left(2\pi m/n\right)e^{\frac{sT_o}{n}}Q(s)-Q^2(s)}{e^{\frac{2sT_o}{n}}-2\cos\left(2\pi m/n\right)e^{\frac{sT_o}{n}}Q(s)+Q^2(s)}$$

where G_f(s) is a phase-lead compensator to stabilize the overall system, and low-pass filter Q(s) is employed to make a good tradeoff between the tracking accuracy and the system robustness as discussed in previous sections.

The SHC module of (10) provide a universal recursive IMP-based controller which is tailored for $nk\pm m$ order harmonics compensation, for example, let n=1 and m=0, (8) becomes a CRC, and let n=4 and m=1, (8) becomes an odd harmonic RC [14]. It is named as "*nk±m order RC*" [14].

In order to compensate more harmonics for better accuracy while keeping fast error convergence rate, an Optimal SHC (OSHC) which includes paralleled SHC modules tailored for the selected harmonics, is proposed as

$$G_{SHC}(s)=\sum_{m\in N_m}G_{nm}(s) \quad (11)$$

where m and N_m represent $nk\pm m$ (k=0,1,2, … and $m\le n/2$) harmonic order and the set of selected harmonics respectively.

The proposed SHC in real form successfully bridges the real "*nk±m order RC*" and the complex "parallel structure RC" [12], [13]. Compared with "parallel structure RC, it at least can reduce the number of SHC modules by half. If equal k_m (m=0,1,2,…, [n/2]) are applied to all SHC modules, OSHC of (11) is actually equivalent to a CRC of (1) with gain $k_{rc}=0.5k_m/n$ [12], [13]. Dual mode structure RC [10], [11] is a special case of OSHC with n=4 and m=0, 1, 2.

III. Digital OSHC System

Fig. 6 shows a typical closed-loop control system with a plug-in SHC controller $G_{SHC}(z)$, where $G_p(z)$ is the transfer function of the plant; $G_c(z)$ is the feedback controller; $G_{SHC}(z)$ is a corresponding digital form OSHC of (11); $r(z)$ is the reference input; $y(z)$ is the output; $e(z)=r(z)-y(z)$ is the tracking error and the input of $G_{SHC}(z)$; $d(z)$ is the disturbance. And the output $y(z)$ of the plug-in SHC system can be expressed as

$$\begin{aligned} y(z) &= G(z)\cdot r(z)+G_d(z)\cdot d(z) \\ &= \frac{\left[1+G_{SHC}(z)\right]H(z)}{1+G_{SHC}(z)H(z)}r(z)+\frac{\left[1+G_c(z)G_p(z)\right]^{-1}}{1+G_{SHC}(z)H(z)}d(z) \end{aligned} \tag{12}$$

where $G(z)$ is the transfer function from $y_d(z)$ to $y(z)$; $G_d(z)$ is the transfer function from $d(z)$ to $y(z)$; $H(z)$ is the transfer function of conventional feedback control system without plug-in OSHC controller $G_{SHC}(z)$. And

$$\begin{aligned} G_{SHC}(z) &= \sum_{m\in N_m} G_{nm}(z) \\ &= \sum_{m\in N_m} k_m \frac{\left[\cos(2\pi m/n)z^{N/n}Q(z)-Q^2(z)\right]G_f(z)}{z^{2N/n}-2\cos(2\pi m/n)z^{N/n}Q(z)+Q^2(z)} \end{aligned} \tag{13}$$

$$H(z)=\frac{G_c(z)G_p(z)}{1+G_c(z)G_p(z)} \tag{14}$$

in which $N=f_s/f_0$ with $f_0=1/T_0$ being the fundamental frequency and f_s being the sampling frequency; k_m is the control gain; $G_f(z)$ is the digital phase compensation filter; $Q(z)$ is the digital low-pass filter with $|Q(e^{j\omega})|\le 1$ is employed to make a good tradeoff between the control accuracy and the system robustness, it removes minor but unexpected high frequency disturbances with $|Q(e^{j\omega})|\to 1$ at low frequencies and $|Q(e^{j\omega})| \to 0$ at high frequencies, *e.g.* $Q(z)=\alpha_1 z+\alpha_0+\alpha_1 z^{-1}$ with $2\alpha_1+\alpha_0=1$, $\alpha_0\ge 0$ and $\alpha_1\ge 0$ [5].

Without loss of generality, $H(z)$ can be described by

$$H(z)=\frac{B(z)}{A(z)}=\frac{z^{-d}B^{+}(z)B^{-}(z)}{A(z)} \tag{15}$$

where d denotes the known delay steps with $d\in[0,N/n]$; all the roots of $A(z)=0$ are inside the unit circle; $B(z)$ and $\left(z^{N/n}-e^{j2\pi m/n}\right)\cdot\left(z^{N/n}-e^{-j2\pi m/n}\right)$ are coprime; $B^{+}(z)$ and $B^{-}(z)$ are the cancellable and un-cancelable parts of $B(z)$ respectively. $B^{-}(z)$ comprises roots on or outside the unit circle and undesirable roots which are in the unit circle and $B^{+}(z)$ comprises roots of $B(z)$ which are not in $B^{-}(z)$.

The compensation filter $G_f(z)$ can be chosen as follows:

$$G_f(z)=\frac{z^d A(z)B^{-}(z^{-1})}{B^{+}(z)b} \tag{16}$$

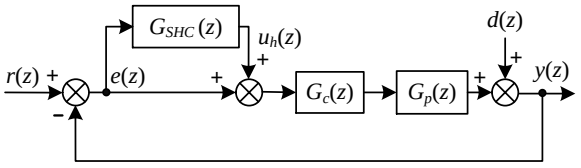

Fig. 6. Digital selective harmonic control system.

where $b\ge\max\left|B^{-}(e^{j\omega})\right|^2$.

The SHC system with $Q(z)$=1 in Fig.4 is asymptotically stable if the following two conditions hold [13], [14]:

1) $H(z)$ is asymptotically stable;
2) Control gains k_m ($\ge$0) satisfy the following inequality:

$$0<\sum_{m\in N_m} k_m<2 \tag{17}$$

Obviously, the above stability criteria for OSHC system can be derived from that for the parallel structure RC system [12], [13], and is compatible to those for other RC systems [4]-[6], [8]-[11], [14]-[21]. It should be noted that OSHC offers power converters an optimal IMP-based control solution to power harmonics compensation: high accuracy, fast transient response, cost-effective and easy real-time implementation, and compatible design rules-of-thumb.

IV. Application Case I: Three-Phase Grid-Connected Inverter Systems

Fig. 7 shows a grid-connected three-phase 6-pulse inverter for PV applications, which is used to feed currents into the grid. The inner current control loop, which comprises a feedback deadbeat and plug-in SHC controller, is used to evaluate the proposed OSHC scheme. The outer control loop, which is responsible for generating accurate current references for the inner control loop, is also shown in Fig. 7.

A. Modeling and Control

As shown in Fig.7, the capacitor C_f for the *LCL*-filter is used to eliminate high-order harmonic currents of the switching frequencies. Together with grid-side inductor L_2, they can be referred to as an "ideal" load, or they can be taken as "model mismatch" [27]. Therefore, the dynamics of the three-phase grid-tied PV inverter shown in Fig. 7 can be simplified into a "*L*"-filter one as below

$$\begin{pmatrix} \dot{i}_a \\ \dot{i}_b \\ \dot{i}_c \end{pmatrix} = \begin{pmatrix} -\frac{R_1}{L_1} & 0 & 0 \\ 0 & -\frac{R_1}{L_1} & 0 \\ 0 & 0 & -\frac{R_1}{L_1} \end{pmatrix} \begin{pmatrix} i_a \\ i_b \\ i_c \end{pmatrix} + \begin{pmatrix} \frac{v_{sa}-v_{an}}{L_1} \\ \frac{v_{sb}-v_{bn}}{L_1} \\ \frac{v_{sc}-v_{cn}}{L_1} \end{pmatrix} \tag{18}$$

where v_{sa}, v_{sb} and v_{sc} are the inverter output voltages, i_a, i_b and i_c are the grid currents, v_{an}, v_{bn}, v_{cn} are the grid voltages, L_1 and R_1 are the nominal values of inverter-side inductor.

The control objective of the inverter is to achieve a unity power factor in normal operation modes, and a low harmonic distortion sinusoidal feeding current. The corresponding sampled-date model of Eq. (18) can be expressed as

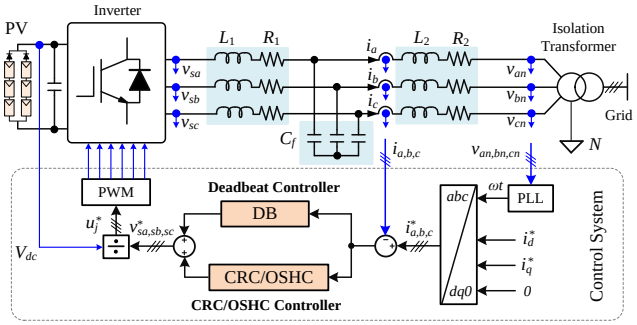

Fig. 7. A selective harmonic controlled three-phase grid-connected inverter system with an *LCL*-filter for PV applications.

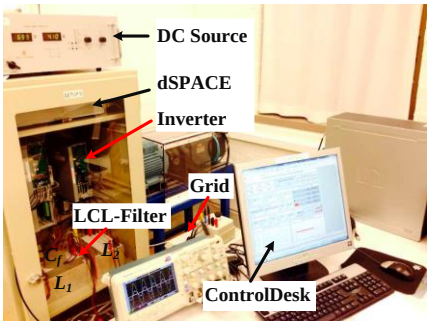

Fig. 8. Experimental setup of a three-phase grid-connected system.

$$i_j(k+1)=\frac{b_1-b_2}{b_1}i_j(k)+\frac{v_{sj}(k)}{b_1}-\frac{v_{jn}(k)}{b_1} \quad (19)$$

$$v_{sj}(k)=u_j(k)\frac{v_{dc}(k)}{2} \quad (20)$$

where the subscript j = a, b, c, b_1=L_1/T_s with T_s being the sampling time, b_2=R_1, v_{dc} is the DC bus voltage, and u_j (u_a, u_b, u_c) are the normalized outputs of the system controller.

If the current controller is chosen for the plant (18) as

$$u_j(k)=\frac{2}{v_{dc}(k)}\left[v_{jn}(k)+b_1 i_{jref}(k)-(b_1-b_2)i_j(k)\right], \quad (21)$$

$i_j(k+1)$ = $i_{jref}(k)$ is obtained, *i.e.* a deadbeat current controller is used. The deadbeat controller is sensitive to the accuracy of the model for the inverter. In practice, it is hard to get an accurate inverter model due to parameter uncertainties and load disturbances. Hence, as shown in Fig. 6, CRC $G_{rc}(z)$ shown in Fig. 2 and the proposed OSHC of (13) are respectively added to ensure accurate current tracking. In both CRC and OSHC, a linear phase-lead filter of $G_f(z)$ = z^p with p being the compensation steps determined by experiments is used to enhance the system performance [17], [18].

B. Experimental Setup

As shown in Fig. 8, a test rig is built-up, where a three-phase commercial power converter is connected to the grid through an *LCL*-filter, and the control system was implemented by using a dSPACE 1103 rapid prototyping kit. Parameters of the test setup are listed in Table I. To achieve approximately zero phase compensation, a filter $G_f(z)$=z^p is used to compensate sampling delays, model mismatches, and un-modeled delay for both CRC and OSHC systems, where the lead step p=3 is determined by experiments.

TABLE I. PARAMETERS OF A THREE-PHASE INVERTER SYSTEM.

LCL-filter	L_1=L_2= 1.8 mH, C_f = 4.7 μF, R_1=R_2= 0.02 Ω
Transformer leakage inductance	L_g= 2 mH per phase
Switching & sampling freq.	f_s = f_{sw} = 9.9 kHz
DC voltage	V_{dc}= 650 V
Nominal grid voltage v_{jn}	50 Hz, 325 V (peak)
Nominal grid current i_j	4.3 A (peak), unity power factor
Repetitive control gain	k_{rc}= 2
SHC control gains	k_0= 0.2, k_1= 1.2, k_2= 0.4, k_3= 0.2

C. Experimental Results

The deadbeat control is firstly tested in order to obtain the harmonic distributions. Fig. 9(a) shows the steady-state responses of grid phases v_{an} and v_{bn}, and the feeding phase current i_a, and the corresponding Fast Fourier Transform (FFT) based harmonic spectrum of current i_a is shown in Fig. 9(b). From the harmonic spectrum shown in Fig. 9(b), it is known that the ratios of all 6k (*i.e.* 0, 6, 12 …) order harmonics, all 6k±1 (*i.e.* 5, 7, 11, …) order harmonics, all 6k±2 (*i.e.* 2, 4, 8, …) order harmonics and all 6k±3 (*i.e.* 3, 9, 15…) order harmonics to the total harmonics are nearly 8.8 %, 60.6 %, 23.7 %, and 6.9 %, respectively. According to the harmonics distribution and (13), an OSHC controller can be employed as

$$G_{SHC}(z)=\sum_{m\in N_m}G_{nm}(z)=G_{60}(z)+G_{61}(z)+G_{62}(z)+G_{63}(z) \quad (22)$$

The corresponding control gains for SHC modules $G_{60}(z)$, $G_{61}(z)$, $G_{62}(z)$, and $G_{63}(z)$ are denoted as k_0, k_1, k_2 and k_3. Since the error convergence rate at any harmonic frequency is proportional to its corresponding control gain, k_0, k_1, k_2 and k_3 are weighted by their ratios in the total harmonics for a better total convergence rate. Thus they satisfy k_3<k_0<k_2<k_1. Furthermore, according to the compatible stability criteria (4) and (17), the stability range of control gain k_{rc} for CRC system is 0<k_{rc}<2 and that for above OSHC system is 0<k_0+k_1+k_2+k_3<2. Therefore k_{rc}=k_0+k_1+k_2+k_3 is used for the comparison of the total error convergence rate between CRC and OSHC in the this case, and the gains are listed in Table I.

To further evaluate the distribution of harmonics magnitudes, the harmonic ratio is denoted as $f(j)$ as below

$$f(j)=\sum_{i=0}^{j}M_i \Big/ \sum_{i=0}^{99}M_i \quad (23)$$

where M_i is the magnitude of the i-th order harmonic. The corresponding harmonic ratio $f(j)$ for the harmonic spectrum of i_a shown in Fig. 9(b) is given in Fig. 10(a), and it indicates that over 85 % of the harmonics are located within a frequency range of 0~2.5 kHz. Therefore, the cut-off frequency f_{cutoff} of low-pass filters (LPFs) $Q(z)$ for CRC and $Q^2(z)$ for OSHC should satisfy f_{cutoff} ≥ 2.5 kHz for the removal of most of the harmonic distortions. As it is shown in Fig. 10(b), the cut-off frequencies of the LPFs, $Q(z)$=0.145z+0.71+0.145z^{-1} and $Q^2(z)$ =(0.075z+0.85+0.075z^{-1})^2 are 2.49 kHz and 2.57 kHz, respectively, and meet approximately the bandwidth requirement.

Fig. 11 shows the steady state response of plug-in CRC controlled converter with k_{rc}=2 and the corresponding harmonic spectrum of the feeding current i_a with THD= 3.12%. Fig. 12 shows the steady-state response of plug-in OSHC controlled converter with k_0=0.2, k_1=1.2, k_2=0.4, k_3=0.2 and the corresponding harmonic spectrum of the feeding

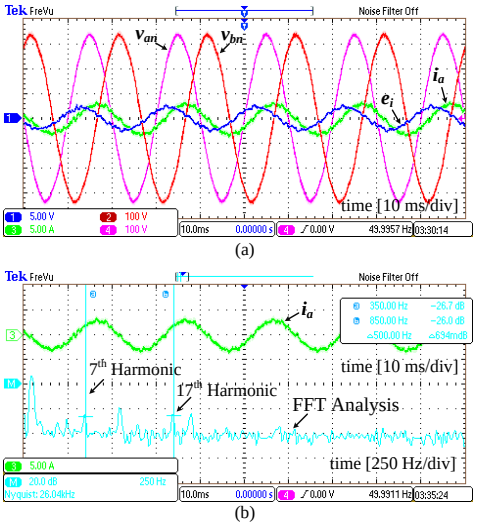

Fig. 9. Steady-state response of a DB controlled three-phase inverter: (a) phase voltages v_{an}, v_{bn} [100 V/div], phase A current i_a [5 A/div] and tracking error e_i=i_{aref}-i_a [5 A/div], and (b) magnitude of current i_a [20 dB/div].

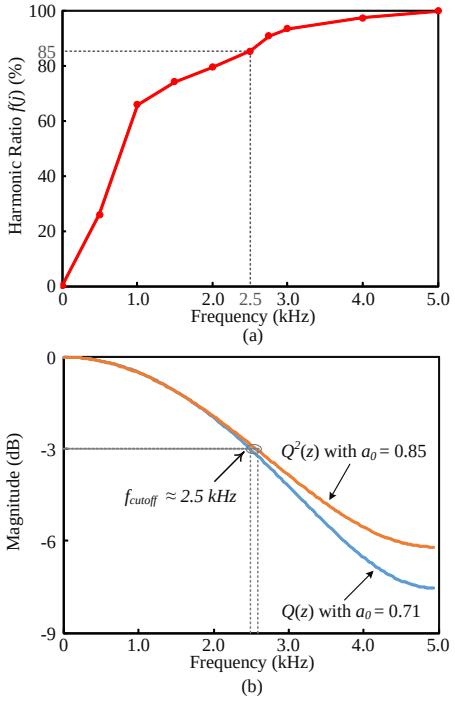

Fig. 10. Spectrum analysis of the phase A current i_a: (a) harmonic ratio $f(j)$ and (b) magnitude response of the LPFs used in CRC and OSHC controllers with f_s = 9.9 kHz.

current i_a with THD = 3.74 %. Figs. 11 and 12 clearly indicate both CRC and OSHC can produce sinusoidal currents with very low THDs in compliance with grid requirements. Fig. 13(a) shows that the setting time for CRC controlled transient tracking current error $e_i(t)$=$i_{aref}(t)$-$i_a(t)$ is about 0.52s, and Fig. 13(b) shows that the setting time for OSHC controlled current error $e(t)$=$i_{aref}(t)$-$i_a(t)$ is about 0.19s. It means that the transient response of proposed OSHC can be much faster (up to n/2 times) than that of CRC. A benchmark of the PV inverter using three different control schemes is shown in Table II and Table III in terms of THD, convergence rate, and harmonic distributions.

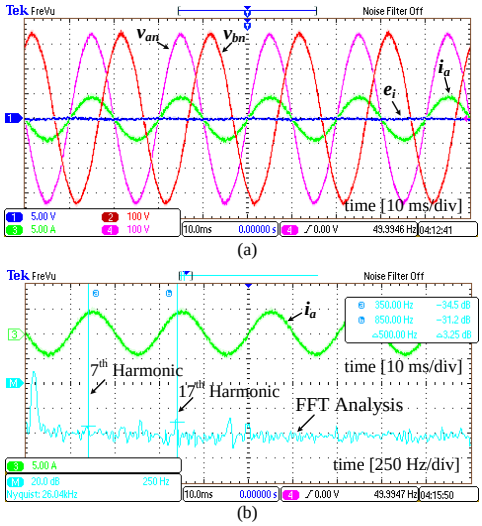

Fig. 11. Steady-state response of CRC controlled three-phase inverter: (a) phase voltages v_{an}, v_{bn} [100 V/div], phase A current i_a [5 A/div] and tracking error e_i=i_{aref}-i_a [5 A/div], and (b) magnitude of current i_a [20 dB/div].

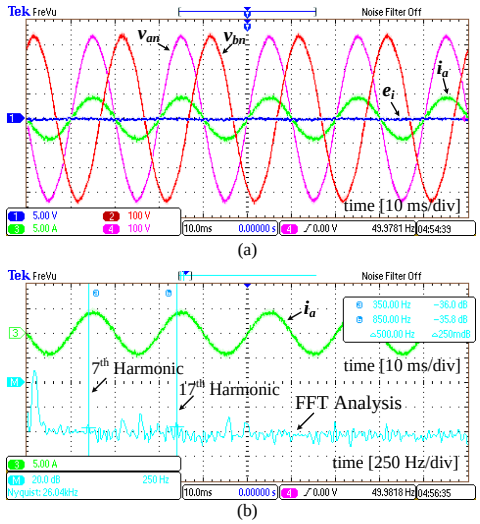

Fig. 12. Steady-state response of OSHC controlled three-phase inverter: (a) phase voltages v_{an}, v_{bn} [100 V/div], phase A current i_a [5 A/div] and tracking error e_i=i_{aref}-i_a [5 A/div], and (b) magnitude of current i_a [20 dB/div].

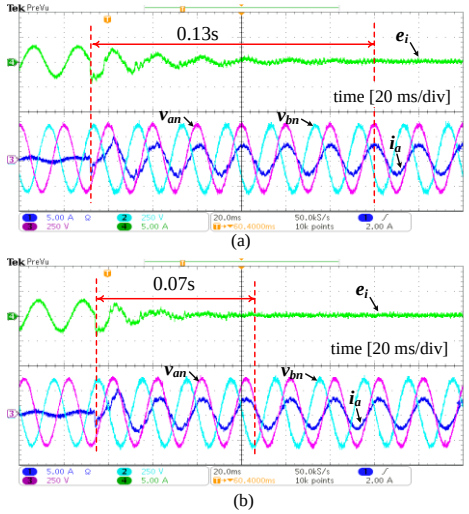

Fig. 13. Transient current tracking errors $e_i(t)$=$i_{aref}(t)$-$i_a(t)$ [2 A/div] of a three-phase grid-connected inverter (grid peak current: 3 A) using different control method: (a) CRC scheme and (b) OSHC scheme.

TABLE II. MAJOR HARMONIC DISTRIBUTION.

Control Schemes	Harmonics to Fundamental (%)							
	2nd	4th	5th	7th	11th	13th	17th	19th
DB	1.67	1.43	1.96	2.79	5.39	1.04	2.95	2.97
DB+ CRC	0.82	0.52	0.27	0.47	0.73	1.55	1.21	0.41
DB+ OSHC	0.81	0.83	0.35	0.57	1.05	1.97	1.46	0.33
Control Schemes	Harmonics to Fundamental (%)							
	23rd	25th	29th	31st	35th	-		
DB	0.76	0.49	0.72	0.59	0.15	-		
DB+ CRC	1.25	0.94	0.17	0.14	0.23	-		
DB+ OSHC	1.24	0.85	0.3	0.12	0.18	-		

TABLE III. PERFORMANCE COMPARISONS.

Control Schemes	THD	Convergence time
DB	8.38 %	-
DB+ CRC	3.12 %	about 0.13s
DB+ OSHC	3.74 %	about 0.07 s

V. APPLICATION CASE II: SINGLE-PHASE GRID-CONNECTED INVERTER SYSTEMS

As shown in Fig. 14, a typical single-phase 1kVA inverter with an *LCL*-filter for PV applications is configured for the test. The proposed OSHC scheme is adopted in the current control loop to guarantee the power quality of the injected grid current within the required range (*e.g.* THD<5%).

A. Modeling and Control

As mentioned in § IV, the capacitor C_f is used to eliminate high-order harmonic currents of switching frequencies, and together with grid-side inductor L_2, it is referred to as an "ideal" load [27]. Hence, the dynamics of the PV inverter in Fig. 14 can simply be described as,

$$L_1\dot{i}_g = -R_1 i_g + \left(v_{inv} - v_g\right) \tag{24}$$

where v_g is the grid voltages, i_g is the grid currents, L_1 and R_1 are the nominal values of ac-side inductor (*LCL*-filter, L_1) and resistor (*LCL*-filter, R_1) respectively.

One control objective of the inverter is to achieve a unity power factor and thus a second-order generalized integrator based phase locked loop (PLL) system is adopted. The second objective is to maintain a low harmonic distortion sinusoidal feeding current using advanced control schemes.

The sampled-date model of (24) can be written as

$$i_g(k+1) = \frac{b_1 - b_2}{b_1} i_g(k) + \frac{u(k)}{b_1} v_{dc}(k) - \frac{v_g(k)}{b_1} \tag{25}$$

where $b_1=L_1/T_s$, $b_2=R_1$, u is the modulation signal with $v_{inv}(t)=u(t)v_{dc}(t)$, and T_s is the sampling period.

For the plant (25), a Dead-Beat (DB) current controller is adopted as,

$$u(k) = \frac{1}{v_{dc}(k)}\left[v_g(k) + b_1 i_{gref}(k) - \left(b_1 - b_2\right) i_g(k)\right] \tag{26}$$

which makes $i_g(k+1)=i_{gref}(k)$. As shown in Fig. 14, the CRC $G_{rc}(z)$ and the proposed OSHC of (13) are respectively plugged into the current control loop to ensure high accuracy current tracking.

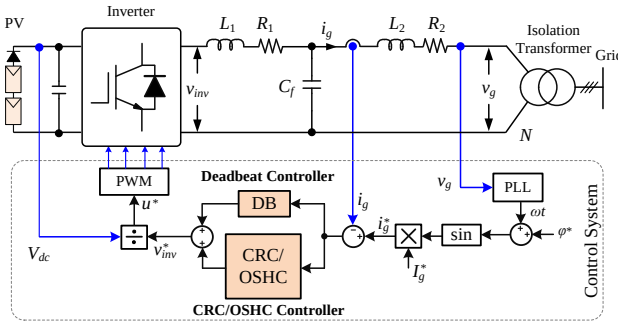

Fig. 14. A selective harmonic controlled single-phase grid-connected inverter with an *LCL*-filter.

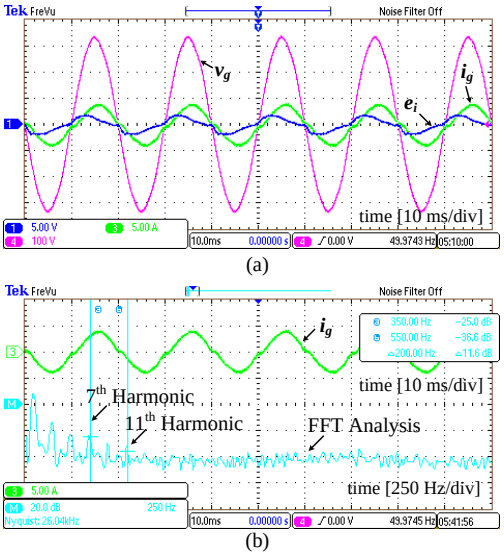

Fig. 15. Steady-state response of DB controlled single-phase inverter: (a) grid voltage v_g [100 V/div], grid current i_g [5 A/div] and tracking error $e_i=i_{gref}-i_g$ [5 A/div], and (b) magnitude of grid current [20 dB/div].

TABLE IV. SYSTEM PARAMETERS.

LCL-filter	$L_1=L_2$=3.6 mH, C_f = 2.35 μF, $R_1=R_2$=0.04 Ω,
Transformer leakage inductance	L_g=2 mH
Switching and sampling frequency	f_{sw}=10 kHz
DC voltage	V_{dc}=400 V
Nominal grid voltage v_g	50 Hz, 325 V (peak)
Nominal grid current i_g	5 A (peak), at unity power factor
Repetitive control gain	k_{rc}=1.8
SHC control gains	k_0= 0.25, k_1= 1.3, k_2= 0.25

B. Experimental Setup

The system parameters for the experimental test rig are listed in Table IV. For both CRC and OSHC, to achieve approximately zero phase compensation, a filter $G_f(z)=z^p$ is used to provide phase-lead compensation, where the lead step p=3 is determined by experiments.

C. Experimental Results

Fig. 15(a) shows the steady-state response of grid voltage v_g and the grid current i_g with DB control according to (26). The corresponding harmonic spectrum of the current i_g, where the harmonic order i=0,2,3,… are shown in Fig. 15(b). A detailed calculation of the harmonic distributions according to (22) shows that the ratios of all 4k (*i.e.* 0, 4, 8 …) order harmonics

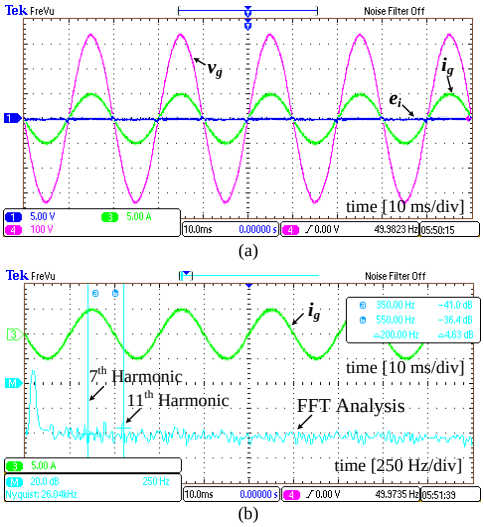

Fig. 16. Steady-state response of CRC controlled grid-connected inverter: (a) grid voltage v_g [100 V/div], grid current i_g [5 A/div] and tracking error e_i=i_{gref}-i_g [5 A/div], and (b) magnitude of grid current [20 dB/div].

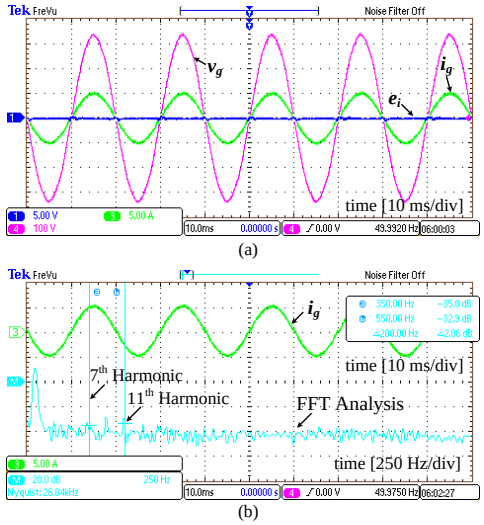

Fig. 17. Steady-state response of OSHC controlled grid-connected inverter: (a) grid voltage v_g [100 V/div], grid current i_g [5 A/div] and tracking error e_i=i_{gref}-i_g [5 A/div], and (b) magnitude of grid current [20 dB/div].

and all $4k\pm2$ (*i.e.* 2, 6, 10, …) order harmonics to the total harmonics are nearly 14.4 % and 14.8 % respectively. Taking account of about 70.7 % of the total harmonics, the dominant harmonics are of $4k\pm1$ (*i.e.* 3, 5, 7, …) order. According to the proposed OSHC of (14) for compensating current harmonic, an OSHC controller can be employed as

$$G_{OSHC}(z)=\sum_{m\in N_m}G_{nm}(z)=G_{40}(z)+G_{41}(z)+G_{42}(z) \quad (28)$$

where the control gains of the corresponding OSHC modules $G_{40}(z)$, $G_{41}(z)$ and $G_{42}(z)$ are denoted as k_0, k_1 and k_2, and $k_0<k_2<k_1$, which are proportional to their ratios in the total harmonics. For comparison, k_{rc}=k_0+k_1+k_2 is set for CRC and OSHC in the this case.

It is calculated from the harmonic distribution shown in Fig. 15(b) that 85% of the harmonics are within the range of 0~2.5 kHz. Similar to the case of three-phase inverter, $Q(z)$= $0.145z+0.71+0.145z^{-1}$ and $Q^2(z)=(0.075z+0.85+0.075z^{-1})^2$ are chosen for CRC and OSHC, respectively. Fig. 16 shows the steady state response of plug-in CRC controlled single-phase

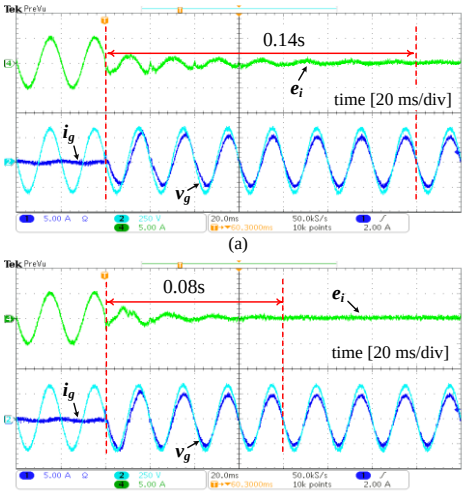

Fig. 18. Transient current tracking errors $e_i(t)$=$i_{gref}(t)$-$i_g(t)$ [2 A/div] of a single-phase grid-connected inverter using different control method: (a) CRC scheme and (b) OSHC scheme.

TABLE V. PERFORMANCE COMPARISONS.

Control Schemes	THD	Convergence time
DB	9.57 %	-
DB+ CRC	2.28 %	about 0.14 s
DB+ OSHC	2.33 %	about 0.08 s

TABLE VI. MAJOR HARMONIC DISTRIBUTION.

Control Schemes	Harmonics to Fundamental (%)								
	2nd	3rd	5th	7th	9th	11th	13th	15th	17th
DB	1.28	8.00	3.43	2.82	1.29	0.88	0.51	0.19	0.38
DB+ CRC	0.10	0.91	0.67	0.61	0.92	0.81	0.54	0.52	0.52
DB+OSHC	0.23	0.68	0.58	0.70	1.03	1.09	0.54	0.67	0.29
Control Schemes	Harmonics to Fundamental (%)								
	19th	21st	23rd	25th	27th	29th	31st	33rd	35th
DB	0.19	0.21	0.25	0.16	0.43	0.5	0.39	0.39	0.38
DB+ CRC	0.21	0.24	0.14	0.06	0.15	0.09	0.15	0.16	0.18
DB+OSHC	0.1	0.15	0.08	0.02	0.17	0.07	0.15	0.19	0.21

inverter with k_{rc}=1.8 and the corresponding harmonic spectrum of feeding current i_g with THD=2.28 %. Fig.17 shows the steady-state response of plug-in OSHC controlled converter with k_0=0.25, k_1=1.3, k_2=0.25 and the corresponding harmonic spectrum of feeding current i_g with THD=2.33 %. Both Figs. 17 and 18 clearly indicate that CRC and OSHC can produce almost perfect sinusoidal currents with very low current THDs. It is shown in Fig. 18(a) that the setting time for CRC controlled transient current tracking error $e_i(t)$=$i_{gref}(t)$-$i_g(t)$ is about 0.47s, while for the OSHC controlled inverter, the convergence time is about 0.34 s as it is shown in Fig. 18(b). It means that transient response of proposed OSHC can be much faster (up to $n/2$ times) than that of CRC, as it is also shown in the benchmarking results in Table V and Table VI in terms of THD, convergence rate, and harmonic distributions. All the experimental tests verified the effectiveness of the proposed current control scheme.

VI. CONCLUSIONS

An IMP-based OSHC method has been proposed in this paper to provide a tailor-made optimal control solution to compensate power harmonics produced by power converters. The hybrid structure enables it to take advantages of both CRC

and MRSC: high accuracy due to the removal of major harmonics, fast transient response due to parallel combination of optimally weighted SHC modules, cost-effective and easy real-time implementation due to the universal recursive SHC modules, and compatible design rules-of-thumb. The analysis and synthesis of the optimal selective harmonic control system have been addressed in this paper. It also provides a universal framework for housing various RC schemes, and successfully bridges the real "*nk±m order RC*" and the complex "parallel structure RC". Two application examples of grid-tied PWM inverters have demonstrated the effectiveness and advantages of the proposed OSHC scheme in suppressing their feeding current harmonics.

REFERENCES

[1] F. Blaabjerg, M. Liserre, R. Teodorescu, A.V. Timbus "Overview of Control and Grid Synchronization for Distributed Power Generation Systems." *IEEE Trans. Ind. Electron.*, vol.53, no.5, pp.1398-1409, 2006.

[2] R. Teodorescu, F. Blaabjerg, M. Liserre, P.C. Loh, "Proportional resonant controllers and filters for grid-connected voltage-source converters," *IEE Proc. Electric Power Appl*,.vol.153, no.5, pp.750-762, Sep. 2006.

[3] M. Liserre, R. Teodorescu, F. Blaabjerg, "Multiple harmonics control for three-phase grid converter systems with the use of PI-RES current controller in a rotating frame." *IEEE Trans. Power Electron.*, vol.21, no.3, pp.836-841, 2006.

[4] K. Zhou, Z. Qiu, N.R. Watson, and Y. Liu, "Mechanism and elimination of harmonic current injection from single-phase grid-connected PWM converters," *IET Power Electronics* vol.6, no.1, pp.88–95, 2013

[5] K. Zhou, D. Wang, "Zero tracking error controller for three-phase CVCF PWM inverter," *Electronics Letters*, vol.36, no.10, pp.864-865, 2000

[6] B. Zhang, K. Zhou, D. Wang, "Multirate Repetitive Control for PWM DC/AC Converters," *IEEE Trans. Ind. Electronics*, vol.61, no.6, pp. 2883-2890, 2014

[7] P. Mattavelli and F. P. Marafao, "Repetitive-based control for selective harmonic compensation in active power filters," *IEEE Trans. Ind. Electron.*, vol. 51, no. 5, pp. 1018-1024, Oct. 2004

[8] R. Costa-Castelló, R. Griñó, E. Fossas. "Odd-harmonic digital repetitive control of a single-phase current active filter." *IEEE Trans. Power Electronics*, vol.19, no.4, pp.1060-1068, 2004

[9] G. Escobar, P.G. Hernandez-Briones, P.R. Martinez, R.E. Torres-Olguin, "A repetitive-based controller for the compensation of 6l±1 harmonic components." *IEEE Trans. Ind. Electron.*, vol.55, no.8, pp.3150-3158, 2008

[10] K. Zhou, D.Wang, B. Zhang, Y. Wang, J.A. Ferreira, and S.W.H. de Haan, "Dual-mode structure digital repetitive control." *Automatica*, vol.43, no.3, pp.546-554, 2007.

[11] K. Zhou, D. Wang, B. Zhang, B. and Y. Wang, "Plug-in dual-mode structure digital repetitive controller for CVCF PWM inverters," *IEEE Tran. Ind. Electron.*, vol.56, no.3, pp.784-791, 2009

[12] W. Lu, K. Zhou, D. Wang. "General parallel structure digital repetitive control." *International Journal of Control*, vol.86, no.1, pp.70-83, 2013.

[13] W. Lu, K. Zhou, D. Wang, and M. Cheng, "A general parallel structure repetitive control scheme for multi-phase DC-AC PWM converters," *IEEE Trans. Power Electronics*, vol.28, no.8, pp.3980-3987, 2013.

[14] W. Lu, K. Zhou, D. Wang, and M. Cheng, "A generic digital nk±m order harmonic repetitive control scheme for PWM converters," *IEEE Trans. Industrial Electronics*, vol.61, no.3, pp.1516-1527, 2014.

[15] Q. C. Zhong and T. Hornik, "Cascaded current–voltage control to improve the power quality for a grid-connected inverter with a local load," *IEEE Trans. Ind. Electron.*, vol. 60, no. 4, pp. 1344-1355, 2013.

[16] W. Zhu, K. Zhou, M. Cheng, "A bidirectional high-frequency-link single-phase inverter: modulation, modeling, and control," *IEEE Trans. on Power Electron.*, vol.29, no.8, pp.4049-4057, 2014

[17] B. Zhang, D. Wang, K. Zhou, Y. Wang. "Linear phase lead compensation repetitive control of a CVCF PWM inverter." *IEEE Trans. Ind. Electron.*, vol.55, no.4, pp.1595-1602, 2008.

[18] B. Zhang, K. Zhou, Y. Wang, and D. Wang, "Performance improvement of repetitive controlled PWM inverters: A phase-lead compensation solution," *International Journal of Circuit Theory and Applications* vol.38, no.5, pp.453-469, 2010

[19] K. Inazuma, H. Utsugi, K. Ohishi, and H. Haga, "High-power-factor single-phase diode rectifier driven by repetitively controlled IPM motor," *IEEE Trans. Ind. Electron.*, vol.60, no.10, pp.4427-4437, 2013.

[20] G. Escobar, P. Mattavelli, M. Hernandez-Gomez, and P. R. Martinez-Rodriguez, "Filters with linear-phase properties for repetitive feedback," *IEEE Trans. Ind. Electron.*, vol.61, no.1, pp.405-413, 2014.

[21] H. Fujimoto, T. Takemura, "High-precision control of ball-screw-driven stage based on repetitive control using *n*-times learning filter," *IEEE Trans. on Ind. Electron.*, vol.61, no.7, pp.3694-3703, 2014.

[22] J. Miret, M. Castilla, J. Matas, J. M. Guerrero, and J. C. Vasquez, "Selective harmonic-compensation control for single-phase active power filter with high harmonic rejection," *IEEE Trans. Ind. Electron.*, vol.56, no.8, pp. 3117-3127, Aug. 2009.

[23] Y. Yang, K. Zhou, M. Cheng, and B. Zhang, "Phase compensation multi-resonant control of CVCF PWM converters," *IEEE Trans. Power Electron.*, vol.28, no.8, pp.3923-3930, 2013

[24] M. Angulo, D. A. Ruiz-Caballero, J. Lago, M. L. Heldwein, and S. A. Mussa, "Active power filter control strategy with implicit closed-loop current control and resonant controller," *IEEE Trans. Ind. Electron.*, vol.60, no 7, pp. 2721-2730, Jul. 2013.

[25] M. Castilla, J. Miret, A. Camacho, J. Matas, L.G. de Vicuna, "Reduction of current harmonic distortion in three-phase grid-connected photovoltaic inverters via resonant current control," *IEEE Trans. on Ind. Electron.*,vol.60, no.4, pp.1464-1472, 2013

[26] M. Angulo, D.A. Ruiz-Caballero, D.A., J. Lago, M.L. Heldwein, S.A. Mussa, "Active power filter control strategy with implicit closed-loop current control and resonant controller," *IEEE Trans. on Ind. Electron.*,vol.60, no.7, pp.2721-2730, 2013

[27] L. Malesani, P. Mattavelli, and S. Buso, "Robust dead-beat current control for PWM rectifiers and active filters," *IEEE Trans. Ind. Appl.*, vol. 35, no. 3, pp. 613-620, May/Jun. 1999.

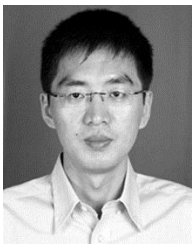

Keliang Zhou (M'04-SM'08) received the B.Sc. degree from the Huazhong University of Science and Technology, Wuhan, China, the M.Eng. degree from Wuhan Transportation University (now the Wuhan University of Technology), Wuhan, and the Ph.D. degree from Nanyang Technological University, Singapore, in 1992, 1995, and 2002, respectively.

During 2003-2006, he was a Research Fellow at Nanyang Technological University in Singapore and at Delft University of Technology in the Netherlands, respectively. From 2006 to 2011, he was with Southeast University, Nanjing, China, as a Professor in the School of Electrical Engineering. Since 2011 he joined the Department of Electrical and Computer Engineering at the University of Canterbury, Christchurch, New Zealand. He has authored or coauthored more than 90 technical papers and several granted patents in relevant areas. His teaching and research interests include power electronics and electric drives, renewable energy generation, control theory and applications, and microgrid technology.

Yongheng Yang (S'12) received the B.Eng. in electrical engineering and automation from North-western Polytechnical University, Xi'an, China, in 2009. During 2009–2011, he was enrolled in a master-doctoral program in the School of Electrical Engineering at Southeast University, Nanjing, China. During that period, he was involved in the modeling and control of single-phase grid-connected photo-voltaic (PV) systems. From March to May in 2013, he was a Visiting Scholar in the Department of Electrical and Computer Engineering at Texas A&M University, College Station, TX, USA. He is currently working toward the Ph.D. degree in the Department of Energy Technology at Aalborg University, Aalborg East, Denmark.

His research interests include grid detection, synchronization, and control of single-phase photovoltaic systems in different operation modes, and reliability for next-generation PV inverters.

Frede Blaabjerg (S'86–M'88–SM'97–F'03) was with ABB-Scandia, Randers, Denmark, from 1987 to 1988. From 1988 to 1992, he was a Ph.D. Student with Aalborg University, Aalborg, Denmark. He became an Assistant Professor in 1992, an Associate Professor in 1996, and a Full Professor of power electronics and drives in 1998. His current research interests include power electronics and its applications, such as in wind turbine systems, PV systems, reliability, harmonics and adjustable speed drives.

He has received 15 IEEE Prize Paper Awards, the IEEE Power Electronics Society (PELS) Distinguished Service Award in 2009, the EPE-PEMC Council Award in 2010, the IEEE William E. Newell Power Electronics Award 2014 and the Villum Kann Rasmussen Research Award 2014. He has served as the Editor-in-Chief of the IEEE TRANSACTIONS ON POWER ELECTRONICS from 2006 to 2012. He has been Distinguished Lecturer for the IEEE Power Electronics Society (PELS) from 2005 to 2007 and for the IEEE Industry Applications Society (IAS) from 2010 to 2011.

Danwei Wang (SM'04) received his Ph.D and MSE degrees from the University of Michigan, Ann Arbor in 1989 and 1984, respectively. He received his B.E degree from the South China University of Tech-nology, China in 1982.

He is professor in the School of Electrical and Electronic Engineering. Nanyang Technological University, Singapore. He is director of EXQUISITUS, Centre for E-City and deputy director of the Robotics Research Centre, NTU. He has served as general chairman, technical chairman and various positions in international conferences. He has served as an Associate Editor of Conference Editorial Board, the IEEE Control Systems Society. He is an Associate Editor of International Journal of Humanoid Robotics and invited guest editor of various international journals. He was a recipient of Alexander von Humboldt Fellowship, Germany. He has published widely in the areas of iterative learning control, repetitive control, fault diagnosis and failure prognosis, satellite formation dynamics and control, as well as manipulator/ mobile robot dynamics, path planning, and control.